

Resolution of Chiral Conundrum in ^{106}Ag : Doppler-Shift Lifetime Investigation

E. O. Lieder,^{1,2} R. M. Lieder,^{1,*} R. A. Bark,¹ Q. B. Chen,³ S. Q. Zhang,³ J. Meng,^{3,4,5} E. A. Lawrie,¹ J. J. Lawrie,¹ S. P. Bvumbi,¹ N. Y. Kheswa,¹ S. S. Ntshangase,¹ T. E. Madiba,¹ P. L. Masiteng,¹ S. M. Mullins,¹ S. Murray,¹ P. Papka,¹ D. G. Roux,⁶ O. Shirinda,¹ Z. H. Zhang,³ P. W. Zhao,³ Z. P. Li,⁷ J. Peng,⁸ B. Qi,⁹ S. Y. Wang,⁹ Z. G. Xiao,^{10,11} and C. Xu³

¹*iThemba LABS, P.O. Box 722, Somerset West 7129, South Africa*

²*Fraunhofer Gesellschaft, Institut für Naturwissenschaftlich-Technische Trendanalysen, D-53881 Euskirchen, Germany*

³*State Key Laboratory of Nuclear Physics and Technology, School of Physics, Peking University, Beijing 100871, China*

⁴*School of Physics and Nuclear Energy Engineering, Beihang University, Beijing 100191, China*

⁵*Department of Physics, University of Stellenbosch, Stellenbosch 7602, South Africa*

⁶*Department of Physics and Electronics, Rhodes University, Grahamstown 6410, South Africa*

⁷*School of Physical Science and Technology, Southwest University, Chongqing 400715, China*

⁸*Department of Physics, Beijing Normal University, Beijing 100875, China*

⁹*Shandong Provincial Key Laboratory of Optical Astronomy and Solar-Terrestrial Environment, School of Space Science and Physics, Shandong University, Weihai 264209, China*

¹⁰*Department of Physics, Tsinghua University, Beijing 100084, China*

¹¹*Collaborative Innovation Center of Quantum Matter, Beijing 100084, China*

(Received 26 December 2013; revised manuscript received 11 March 2014; published 20 May 2014)

The nature of the chiral candidate bands in ^{106}Ag , one of only two known examples of candidates which actually cross, is investigated experimentally and theoretically. Lifetimes have been determined for these bands in ^{106}Ag using the Doppler-shift attenuation method with the γ -detector array AFRODITE. The level scheme of ^{106}Ag has been extended, and three negative-parity bands have been observed to high spins. Configurations were assigned to the negative-parity bands based on a quasiparticle alignment analysis and on configuration-fixed constrained relativistic mean field calculations. The excitation energies, $B(M1)$ and $B(E2)$ values, as well as $B(M1)/B(E2)$ ratios have been compared with results of particle-rotor model calculations. From the investigations, it is concluded that the three close-lying negative-parity bands are a two-quasiparticle high- K band and a pair of four-quasiparticle bands. The proposal that the two lowest-lying bands are chiral partners has not been confirmed.

DOI: 10.1103/PhysRevLett.112.202502

PACS numbers: 21.10.-k, 21.10.Re, 21.10.Tg, 27.60.+j

Spontaneous chiral-symmetry breaking is a phenomenon of general interest, affecting, e.g., the chiral symmetry of the gauge theory in particle physics and the geometric properties of certain molecules in chemistry. Frauendorf and Meng [1] suggested the existence of this phenomenon in triaxial, odd-odd nuclei where three angular momentum vectors may couple to each other in either a left- or right-handed mode. In the laboratory frame, the restoration of spontaneous chiral-symmetry breaking can be observed as a pair of nearly degenerate bands. At low spins, they are energetically separated and understood as a chiral vibrational mode [2,3]. With increasing spin, they approach each other and become approximately degenerate after a critical spin, comprising levels of identical spin and parity, forming thus the static chiral mode—a consequence of quantum tunneling between the left- and right-handed solutions [2,3]. The existence of chiral bands has been proposed in the $A \approx 80$ [4], 100 [5], 130 [6], and 190 [7,8] mass regions.

Although the chiral-partner bands have energies close to each other, it is rare to observe a crossing between them. Crossings are important as a test of the onset of static chirality. The most famous example of such a crossing is in

^{134}Pr [9,10]. Indeed, for some time, ^{134}Pr was regarded as the best example of nuclear chirality.

Additional characteristics of chiral-partner bands are that their in-band $B(M1)$ and $B(E2)$ values as well as their $B(M1)/B(E2)$ ratios should be identical [11,12]. The importance of the investigation of electromagnetic transition rates was demonstrated when measurements revealed large differences in $B(E2)$ values between the candidate chiral bands in ^{134}Pr , causing this nucleus to lose its status as the best example of nuclear chirality [13]. Convincing evidence for the manifestation of static chirality in the $A \approx 130$ region has been found on the basis of lifetime measurements in the nuclei $^{126,128}\text{Cs}$ [14,15].

The only other known case of a crossing between chiral partners is in the nucleus ^{106}Ag , as proposed by Joshi *et al.* [16], where a pair of negative-parity bands crosses at $I = 14$. Such a crossing has not been observed in other doublet bands in the $A \approx 100$ region [5,17–21]. Joshi *et al.* [16] assigned $\pi g_{9/2}^{-1} \otimes \nu h_{11/2}$ configurations to the two lowest negative-parity bands 1 and 2 and considered the effect of large γ softness on the chiral geometry. In a novel suggestion, for the yrast band 1, the nucleus was assumed

to have a triaxial shape, while the excited partner band 2 was explained in terms of an axial nuclear shape. Shape transformation induced by chiral vibration was given as possible explanation for a planar axial rotational band being a partner of a triaxial band. Alternatively, in a recent investigation, Ma *et al.* [22] proposed that the excited partner band 2 in ^{106}Ag is due to the alignment of an extra pair of $h_{11/2}$ neutrons.

With the characterization of the crossing bands being an open question, we have performed a detailed and complete spectroscopic investigation of ^{106}Ag . To provide a stringent test of the chiral interpretation, the lifetimes, hitherto unavailable in the band crossing region, were measured for the bands in ^{106}Ag to high spins using the Doppler-shift attenuation method. In a previous lifetime investigation using the recoil-distance method [23], only lifetimes for band 1 up to $I = 13$, below the crossing region, have been extracted. The present experiment was carried out with the γ -detector array AFRODITE at iThemba LABS, which was equipped with four CLOVER detectors, each at 45° and 135° with respect to the beam direction. A $^{96}\text{Zr}(^{14}\text{N}, 4n)$ reaction at a beam energy of 71 MeV has been used. The target was a self-supporting metallic ^{96}Zr foil of 17 mg/cm^2 thickness with an enrichment of 57.4%. This target thickness was chosen to stop the recoils, which had a maximum initial recoil velocity of $v_o/c = 1.3\%$, in the target. Approximately 3.4×10^9 suppressed γ - γ events were collected.

The level scheme was investigated by replacing the 17 mg/cm^2 target with one of 0.7 mg/cm^2 and collecting approximately 0.4×10^9 γ - γ events. In a second experiment, a stack of two self-supporting ^{96}Zr foils, 0.6 mm apart, with a total thickness of 1.4 mg/cm^2 , was used at a beam energy of 62 MeV. To obtain information on the angular distributions and linear polarizations of the emitted γ radiation, the CLOVER detectors were placed at 45° and 90° , respectively. Approximately 1.1×10^9 suppressed γ - γ coincidence events were collected.

A partial level scheme of ^{106}Ag resulting from the present experiments is shown in Fig. 1. It has been considerably extended with respect to the schemes published in Refs. [16,24,25]. Band 2 has been extended by three transitions up to the 22^- state. Band 3, established up to the 21^- level, has been completely revised with respect to the level scheme of Ref. [24] and is found to deexcite by six newly established high-energy transitions to band 1 (carrying $\approx 80\%$ of the total intensity) and by four transitions to positive-parity states. A $\pi g_{9/2}^{-1/2} \otimes \nu g_{7/2}$ configuration has previously been assigned to the latter states [26]. Spin-parity and multipolarity assignments, based on results of the angular distribution and linear polarization analysis, agree with those given previously [16,24], except for the revised band 3. For this band, a spin and parity of 10^- is assigned to its lowest observed level.

To extract lifetimes, single-gated coincidence spectra from the thick-target experiment have been used. The data

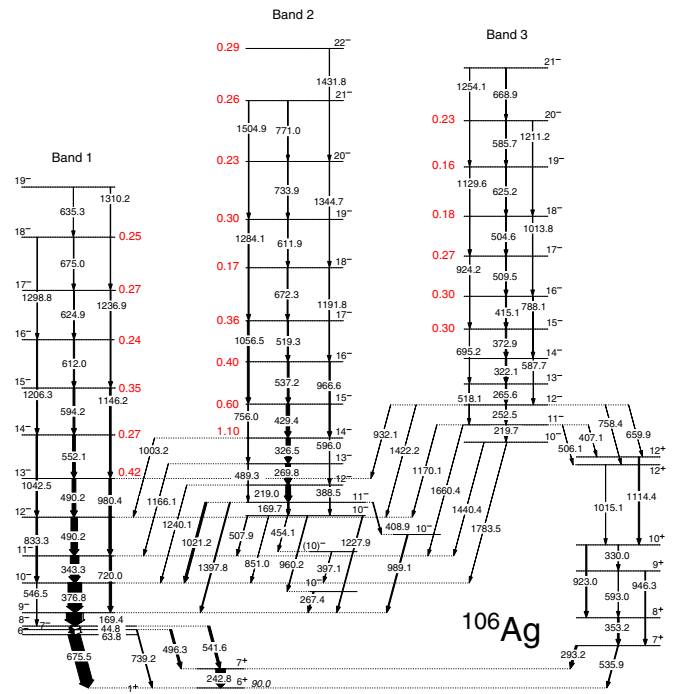


FIG. 1 (color online). Partial level scheme of ^{106}Ag . The widths of the arrows represent the relative intensities of the transitions. The lifetimes in ps, deduced in the present work, are indicated; their uncertainties are, on average, 20%.

were sorted into two γ - γ matrices for which the energies of γ rays detected in the 45° and 135° detectors, respectively, were stored into one axis and those of γ rays observed in any detector into the second axis. For the lifetime analysis, the program system COMPA, GAMMA, SHAPE [27–29] has been used, applying the “wide gate on transition below” gating technique. This requires the knowledge of cascade and sidefeeding intensities. Furthermore, an appropriate treatment of sidefeeding is required to determine its time distribution. The sidefeeding cascades between the entry states of the final nucleus and the considered levels have been simulated with Monte Carlo methods [27–29], taking into account statistical $E1$, $M1$, and $E2$ transitions, stretched $E2$ bands, as well as bands of large deformation in the continuum and particle-hole excitations which generate cascades of stretched magnetic dipole transitions. Parameters for the calculations have been taken from the literature [30,31] or were extracted from the present data set. The effective quadrupole moments $Q_{\text{low}} = 4.0^{+0.8}_{-0.4}$ and $Q_{\text{high}} = 9^{+5}_{-2}$ of the unobserved stretched $E2$ cascades feeding low- and high-spin states, respectively [27], have been determined by line-shape analysis of the strong high-lying $1284.1\text{ keV } 19^- \rightarrow 17^-$ transition of band 2. The deduced quadrupole moments are consistent with experimental values found in ^{105}Ag [32] and ^{108}Cd [33].

The lifetime analysis has been carried out step by step, starting at the highest level in each band, for which a Doppler line shape has been observed. In this way, the

cascade feeding times as well as the sidefeeding time distributions could be taken into account. As an example, the line-shape analysis of the 966.6 keV γ line deexciting the 16^- level of band 2 in ^{106}Ag is shown in Fig. 2. This line shows a broad Doppler line shape and is superimposed by the strong 960.2 keV transition of the instrumental line shape, deexciting the 10^- level of band 2. Taking into account the line-shape analysis of the 537.2 keV transition deexciting the same level, a lifetime of $\tau = 0.40 \pm 0.04$ ps has been deduced for the 16^- level of band 2 in a χ^2 analysis. The uncertainty includes the statistical uncertainty, that related to the cascade and sidefeeding pattern and the uncertainty of the stopping power of the recoils being $\approx 10\%$ [34]. The lifetimes of all investigated levels are given in the level scheme of Fig. 1. From the lifetimes and the branching ratios of the $\Delta I = 1$ and 2 transitions in bands 1 to 3 of ^{106}Ag , the reduced transition probabilities $B(M1)$ and $B(E2)$ have been deduced and are shown in Fig. 3. The $E2:M1$ mixing ratios δ of the $\Delta I = 1$ transitions, deduced in this work, are small and could be neglected in the calculation of the $B(M1)$ values.

Joshi *et al.* [16] have assigned $\pi g_{9/2}^{-1} \otimes \nu h_{11/2}$ configurations to the negative-parity bands 1 and 2, while Ma *et al.* [22] assigned a $\pi g_{9/2}^{-1} \otimes \nu h_{11/2}^3$ configuration to band 2. An inspection of the aligned angular momenta (alignments) reveals that band 1 has $\approx 6\hbar$ while band 2, as well as band 3, have $\approx 10\hbar$, as can be seen in Fig. 4. The different alignments were explained by Joshi *et al.* [16] as a result of aplanar and planar rotations for the partner bands, but here, the alternative of different configuration assignments is

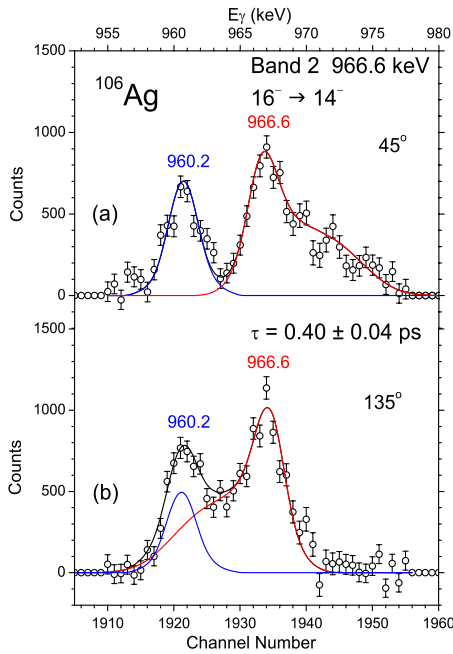


FIG. 2 (color online). The line-shape analysis of the 966.6 keV γ line deexciting the 16^- level of band 2 in ^{106}Ag is shown for (a) the 45° spectrum (forward direction) and (b) the 135° spectrum (backward direction).

considered by performing an empirical analysis of quasiparticle energies e' and alignments i [35]. The quasiparticle alignments i of bands 1 to 3 in ^{106}Ag are compared in Fig. 4 with those obtained by summing quasiparticle alignments of bands from the neighboring odd-mass nuclei ^{105}Ag [20], ^{107}Ag [24], ^{105}Pd [36,37], and ^{107}Cd [38].

As can be seen in Fig. 4(a), the $\pi g_{9/2}^{-1} \otimes \nu h_{11/2}$ configuration assignment to band 1 in ^{106}Ag is confirmed below 0.5 MeV. Above 0.5 MeV, the alignment of band 1 indicates an onset of band crossing.

For bands 2 and 3, a good agreement is found for the alignment if a $\pi g_{9/2}^{-1} \otimes \nu \{g_{7/2}, d_{5/2}\}^2 \nu h_{11/2}$ four-quasiparticle configuration is assigned to the bands where the notation $\nu \{g_{7/2}, d_{5/2}\}$ indicates that the $2d_{5/2}$ and $1g_{7/2}$ neutron orbitals interact and mix with each other. In Fig. 4(b), the alignments of bands 2 and 3 in ^{106}Ag are compared with those deduced from neighboring odd-mass nuclei, using bands C and D in ^{105}Ag of $\pi g_{9/2}^{-1} \otimes \nu \{g_{7/2}, d_{5/2}\} \nu h_{11/2}$ configurations [20]. As can be seen, not only the aligned angular momenta of band 2 in ^{106}Ag but also those of band 3 are quite well reproduced. The alternative $\pi g_{9/2}^{-1} \otimes \nu h_{11/2}^3$ configuration assignment for these bands, proposed by Ma *et al.* [22], can be excluded

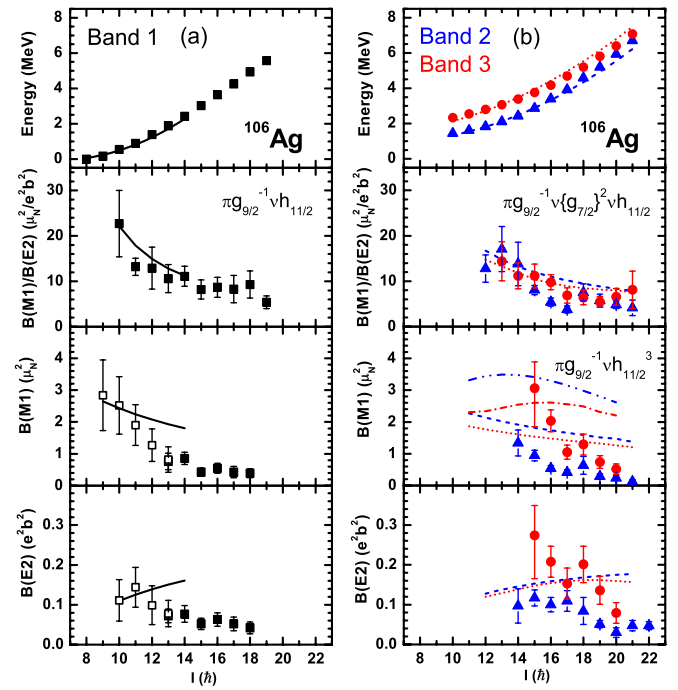


FIG. 3 (color online). Comparison of experimental (symbols) and calculated (lines) excitation energies and electromagnetic transition properties of (a) band 1 and (b) bands 2 and 3. The open squares for band 1 indicate results from Ref. [23]. The theoretical results for $\pi g_{9/2}^{-1} \otimes \nu \{g_{7/2}, d_{5/2}\}^2 \nu h_{11/2}$ configurations of bands 2 and 3 are displayed as dashed and dotted lines, respectively. The $B(M1)$ values of bands 2 and 3 are also compared with calculations using a $\pi g_{9/2}^{-1} \otimes \nu h_{11/2}^3$ configuration, shown as dash-dot-dotted and dash-dotted lines, respectively.

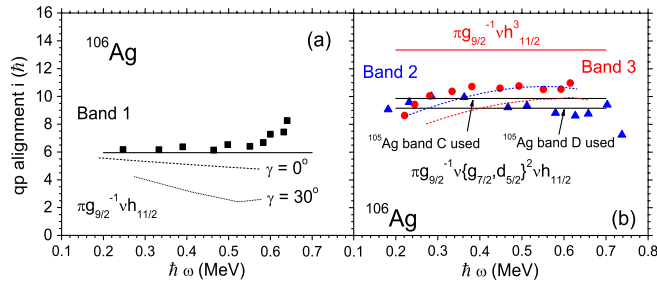


FIG. 4 (color online). Quasiparticle alignment i as function of rotational frequency for (a) band 1 and (b) bands 2 and 3 in ^{106}Ag . The experimental points are shown as full symbols. The alignments deduced from the neighboring nuclei are indicated as straight lines. Results of theoretical calculations are displayed as dashed and dotted lines. The Harris parameters used are $\mathcal{J}_0 = 8.9\hbar^2/\text{MeV}$ and $\mathcal{J}_1 = 15.7\hbar^4/\text{MeV}^3$ [39].

because its alignment is $\approx 3\hbar$ larger than those of bands 2 and 3 [cf. Fig. 4(b)]. This is a significant difference, considering that in the neighboring nuclei, the alignment relations are fulfilled to within $(1-2)\hbar$ [39].

Adiabatic and configuration-fixed constrained triaxial relativistic mean field calculations [40–44] have been carried out with the effective interaction PC-PK1 [45], to find the ground state and the local minima for the negative-parity configurations available in ^{106}Ag . The features for the configurations of these minima are summarized in Table I. The ground state A has a prolate configuration ($\beta = 0.19$, $\gamma = 0^\circ$) and shows softness to γ deformation. State a corresponds to a bandhead of $\pi g_{9/2}^{-1} \otimes \nu h_{11/2}$ configuration, the same as assigned in the quasiparticle analysis to band 1, with a deformation of ($\beta = 0.22$, $\gamma = 0^\circ$). State b corresponds to a bandhead of $\pi g_{9/2}^{-1} \otimes \nu \{d_{5/2}, g_{7/2}\}^2 \nu h_{11/2}$ configuration, the same as assigned in the quasiparticle analysis to bands 2 and 3, with a slight triaxial deformation of ($\beta = 0.21$, $\gamma = 5.3^\circ$). Bands of $\pi g_{9/2}^{-1} \otimes \nu \{g_{7/2}, d_{5/2}\}^2 \nu h_{11/2}$ configuration are indeed expected at low excitation energies theoretically.

To gain a better understanding of the excitation energies and electromagnetic transition properties of bands 1 to 3, particle-rotor model (PRM) calculations using the configurations and deformations given in Table I have been carried out.

For band 1, a moment of inertia of $16\hbar^2/\text{MeV}$ has been used. The calculations reproduce the data well up to

$I = 14$, as shown in Fig. 3(a). The $B(E2)$ value is almost constant because the deformation is fixed in the calculations. Above $I = 14$, band 1 is crossed by a band of $\pi g_{9/2}^{-1} \otimes \nu h_{11/2}^3$ configuration, which is not taken into account in the calculations. Band 1 is at low spins interpreted as a two-quasiparticle high- K band of $\pi g_{9/2}^{-1} \otimes \nu h_{11/2}$ configuration.

The scenario proposed by Joshi *et al.* [16], that bands 1 and 2 have $\pi g_{9/2}^{-1} \otimes \nu h_{11/2}$ configurations of triaxial and prolate shape, can be tested in the model against the experimental alignments. Calculations have been carried out for $\gamma = 0^\circ$ and 30° shown as dotted and dashed curves, respectively, in Fig. 4(a). The $\gamma = 0^\circ$ curve reproduces the experimental alignments reasonably well, while a reduction in aligned angular momentum is predicted for $\gamma = 30^\circ$. Neither curve is in agreement with the larger aligned angular momenta observed for bands 2 and 3.

In the calculations for bands 2 and 3 of $\pi g_{9/2}^{-1} \otimes \nu \{g_{7/2}, d_{5/2}\}^2 \nu h_{11/2}$ configuration, four single- j shells, viz. $1g_{9/2}$, $1h_{11/2}$, $1g_{7/2}$, and $2d_{5/2}$, should be adopted for the PRM calculations, which demands a large model space and a considerable numerical effort. Considering the strong mixing of the $g_{7/2}$ and $d_{5/2}$ pseudospin partner orbitals, the $\{g_{7/2}, d_{5/2}\}^2$ configuration can be well approximated either by a $\{g_{7/2}\}^2$ or a $\{d_{5/2}\}^2$ configuration. The moment of inertia was taken as $22\hbar^2/\text{MeV}$. In Fig. 3(b), the experimental energy and electromagnetic transition properties of bands 2 and 3 in ^{106}Ag are compared with the PRM results. Similar results have been obtained, by using either the $\{g_{7/2}\}^2$ or the $\{d_{5/2}\}^2$ configuration, which demonstrates that the considered approximation is reasonable.

Bands 2 and 3 are separated by ≈ 900 keV at $I \leq 15\hbar$ and gradually approach each other to ≈ 450 keV at $I = 21\hbar$. The experimental and theoretical excitation energies show an impressive agreement. The calculated aligned angular momenta are also in good agreement with experiment, as shown in Fig. 4(b). The experimental $B(M1)/B(E2)$ ratios are reproduced quite well by the PRM calculations, although the agreement between the experimental and calculated $B(M1)$ values, while reasonable, is not as good. Nevertheless, the agreement is clearly better than with the calculated $B(M1)$ values for the alternative, $\pi g_{9/2}^{-1} \otimes \nu h_{11/2}^3$ configuration [cf. Fig. 3(b)],

TABLE I. Excitation energies E_x in MeV, deformation parameters β and γ , unpaired nucleon configurations, as well as parities for the minima of the ground state (gs) A and the negative-parity states a and b in the configuration-fixed constrained triaxial relativistic mean field calculations.

State	E_x	(β, γ)	Unpaired nucleon configuration	π	Experiment
A	0.00	(0.19, 0.0°)	$\pi g_{9/2}^{-1} \otimes \nu g_{7/2}^{-1}$	+	gs
a	1.32	(0.22, 0.0°)	$\pi g_{9/2}^{-1} \otimes \nu h_{11/2}$	-	Band 1
b	1.78	(0.21, 5.3°)	$\pi g_{9/2}^{-1} \otimes \nu \{d_{5/2}, g_{7/2}\}^2 \nu h_{11/2}$	-	Bands 2 and 3

which has already been excluded on the basis of aligned angular momenta.

The observations that the $B(M1)$ values calculated for the $\pi g_{9/2}^{-1} \otimes \nu g_{7/2}^2 \nu h_{11/2}$ configuration do not fall off as quickly with spin as the experimental values and that the calculated $B(E2)$ values increase slightly result from the fact that a frozen rotor is adopted in the calculations. Both the large energy differences between the doublet bands 2 and 3 as well as the small triaxial deformation do not support static chirality [46]. It might be possible to interpret these bands as a pair of four-quasiparticle chiral vibrational bands, considering the γ softness of ^{106}Ag , or alternatively, as pseudospin partner bands, considering that the $g_{7/2}$ and $d_{5/2}$ orbitals are pseudospin partners, but the correct interpretation of bands 2 and 3 requires further investigations.

In summary, a thorough spectroscopic and theoretical investigation of the negative-parity bands in ^{106}Ag has been carried out. The bands have been revised and extended, and their lifetimes were measured using the Doppler-shift attenuation method, representing the first high-quality lifetime measurement of the proposed chiral bands in the mass $A \approx 100$ region. The analysis of alignments and comparison of theoretical and experimental results allow a new understanding of the conundrum represented by the crossing bands 1 and 2. We find that while band 1 corresponds to a $\pi g_{9/2}^{-1} \otimes \nu h_{11/2}$ two-quasiparticle configuration, band 2 neither has a two-quasiparticle configuration nor results from the alignment of a pair of $h_{11/2}$ neutrons [22]. It is conclusive that bands 1 and 2 do not form a pair of chiral-partner bands as proposed by Joshi *et al.* [16].

The crossing between bands 1 and 2 is caused by configurations of different alignment. Although their electromagnetic properties are not fully understood, bands 2 and 3 are in reasonable agreement with the properties expected for $\pi g_{9/2}^{-1} \otimes \nu \{d_{5/2}, g_{7/2}\}^2 \nu h_{11/2}$ four-quasiparticle configurations.

The authors thank the iThemba LABS technical staff and accelerator group for their support. Furthermore, the support of Ch. Droste in the interpretation of the polarization data is gratefully acknowledged. R.M.L. wants to thank iThemba LABS and the Peking University for financial support during short-term stays at iThemba LABS and the State Key Laboratory of Nuclear Physics and Technology, respectively. This work was supported by the National Research Foundation of South Africa, the Major State 973 Program of China (Grant No. 2013CB834400), the Natural Science Foundation of China (Grants No. 11175002, No. 11175108, No. 11335002, and No. 11375015), the Research Fund for the Doctoral Program of Higher Education (Grant No. 20110001110087), the China Postdoctoral Science Foundation (Grants No. 2012M520101 and No. 2013M540011), and the South Africa-China Research Collaboration in Science and Technology (Grant No. CS05-L06).

*Corresponding author.

rainer_lieder@yahoo.com

- [1] S. Frauendorf and J. Meng, *Nucl. Phys.* **A617**, 131 (1997).
- [2] B. Qi, S. Q. Zhang, J. Meng, S. Y. Wang, and S. Frauendorf, *Phys. Lett. B* **675**, 175 (2009).
- [3] S. Mukhopadhyay, D. Almehed, U. Garg, S. Frauendorf, T. Li, P. V. Madhusudhana Rao, X. Wang, S. S. Ghugre, M. P. Carpenter, S. Gros, A. Hecht, R. V. F. Janssens, F. G. Kondev, T. Lauritsen, D. Seweryniak, and S. Zhu, *Phys. Rev. Lett.* **99**, 172501 (2007).
- [4] S. Y. Wang *et al.*, *Phys. Lett. B* **703**, 40 (2011).
- [5] C. Vaman, D. B. Fossan, T. Koike, K. Starosta, I. Y. Lee, and A. O. Macchiavelli, *Phys. Rev. Lett.* **92**, 032501 (2004).
- [6] K. Starosta, T. Koike, C. J. Chiara, D. B. Fossan, D. R. LaFosse, A. A. Hecht, C. W. Beausang, M. A. Caprio, J. R. Cooper, R. Krücken, J. R. Novak, N. V. Zamfir, K. E. Zyranski, D. J. Hartley, D. L. Balabanski, Jing-ye Zhang, S. Frauendorf, and V. I. Dimitrov, *Phys. Rev. Lett.* **86**, 971 (2001).
- [7] E. A. Lawrie, P. A. Vymers, J. J. Lawrie, Ch. Vieu, R. A. Bark, R. Lindsay, G. K. Mabala, S. M. Maliage, P. L. Masiteng, S. M. Mullins, S. H. T. Murray, I. Ragnarsson, T. M. Ramashidzha, C. Schück, J. F. Sharpey-Schafer, and O. Shirinda, *Phys. Rev. C* **78**, 021305(R) (2008).
- [8] P. L. Masiteng *et al.*, *Phys. Lett. B* **719**, 83 (2013).
- [9] C. M. Petrache, D. Bazzacco, S. Lunardi, G. de Angelis, C. Rossi Alvarez, D. Bucurescu, C. R. Ur, and R. Wyss, *Nucl. Phys.* **A597**, 106 (1996).
- [10] K. Starosta, T. Koike, C. J. Chiara, D. B. Fossan, D. R. LaFosse, A. A. Hecht, C. W. Beausang, M. A. Caprio, J. R. Cooper, R. Krücken, J. R. Novak, N. V. Zamfir, K. E. Zyranski, D. J. Hartley, D. L. Balabanski, Jing-ye Zhang, S. Frauendorf, and V. I. Dimitrov, *Phys. Rev. Lett.* **86**, 971 (2001).
- [11] T. Koike, K. Starosta, and I. Hamamoto, *Phys. Rev. Lett.* **93**, 172502 (2004).
- [12] S. Y. Wang, S. Q. Zhang, B. Qi, and J. Meng, *Chin. Phys. Lett.* **24**, 664 (2007).
- [13] D. Tonev *et al.*, *Phys. Rev. Lett.* **96**, 052501 (2006).
- [14] E. Grodner, J. Srebrny, A. A. Pasternak, I. Zalewska, T. Morek, C. Droste, J. Mierzejewski, M. Kowalczyk, J. Kownacki, M. Kisieliński, S. G. Rohoziński, T. Koike, K. Starosta, A. Kordyasz, P. J. Napiorkowski, M. Wolińska-Cichocka, E. Ruchowska, W. Płóciennik, and J. Perkowski, *Phys. Rev. Lett.* **97**, 172501 (2006).
- [15] E. Grodner, I. Sankowska, T. Morek, S. G. Rohoziński, Ch. Droste, J. Srebrny, A. A. Pasternak, M. Kisieliński, M. Kowalczyk, J. Kownacki, J. Mierzejewski, A. Król, and K. Wrzosek, *Phys. Lett. B* **703**, 46 (2011).
- [16] P. Joshi, M. P. Carpenter, D. B. Fossan, T. Koike, E. S. Paul, G. Rainovski, K. Starosta, C. Vaman, and R. Wadsworth, *Phys. Rev. Lett.* **98**, 102501 (2007).
- [17] J. Timár, C. Vaman, K. Starosta, D. B. Fossan, T. Koike, D. Sohler, I. Y. Lee, and A. O. Macchiavelli, *Phys. Rev. C* **73**, 011301(R) (2006).
- [18] J. Timár *et al.*, *Phys. Lett. B* **598**, 178 (2004).
- [19] P. Joshi *et al.*, *Phys. Lett. B* **595**, 135 (2004).
- [20] J. Timár, T. Koike, N. Pietralla, G. Rainovski, D. Sohler, T. Ahn, G. Berek, A. Costin, K. Dusling, T. C. Li,

- E. S. Paul, K. Starosta, and C. Vaman, *Phys. Rev. C* **76**, 024307 (2007).
- [21] P. Joshi, A. R. Wilkinson, T. Koike, D. B. Fossan, S. Finnigan, E. S. Paul, P. M. Raddon, G. Rainovski, K. Starosta, A. J. Simons, C. Vaman, and R. Wadsworth, *Eur. Phys. J. A* **24**, 23 (2005).
- [22] H. L. Ma, S. H. Yao, B. G. Dong, X. G. Wu, H. Q. Zhang, and X. Z. Zhang, *Phys. Rev. C* **88**, 034322 (2013).
- [23] A. I. Levon, J. de Boer, A. A. Pasternak, and D. A. Volkov, *Z. Phys. A* **343**, 131 (1992).
- [24] D. Jerrestam, W. Klamra, J. Gizon, F. Lidén, L. Hildingsson, J. Kownacki, Th. Lindblad, and J. Nyberg, *Nucl. Phys. A* **577**, 786 (1994).
- [25] C. Y. He, L. H. Zhu, X. G. Wu, S. X. Wen, G. S. Li, Y. Liu, Z. M. Wang, X. Q. Li, X. Z. Cui, H. B. Sun, R. G. Ma, and C. X. Yang, *Phys. Rev. C* **81**, 057301 (2010).
- [26] R. Popli, F. A. Rickey, L. E. Samuelson, and P. C. Simms, *Phys. Rev. C* **23**, 1085 (1981).
- [27] E. O. Lieder *et al.*, *Eur. Phys. J. A* **35**, 135 (2008).
- [28] R. M. Lieder *et al.*, *Eur. Phys. J. A* **21**, 37 (2004).
- [29] E. Grodner, A. A. Pasternak, Ch. Droste, T. Morek, J. Srebrny, J. Kownacki, W. Plóciennik, A. A. Wasilewski, M. Kowalczyk, M. Kisieliński, R. Kaczarowski, E. Ruchowska, A. Kordyasz, and M. Wolińska, *Eur. Phys. J. A* **27**, 325 (2006).
- [30] T. Belgya, O. Bersillon, R. Capote Noy, T. Fukahori, G. Zhigang, S. Goriely, M. Herman, A. V. Ignatyuk, S. Kailas, A. J. Koning, P. Oblozinsky, V. Plujko, and P. G. Young, *Handbook for Calculations of Nuclear Reaction Data, RIPL-2*, IAEA-TECDOC-1506 (IAEA, Vienna, 2006).
- [31] R. M. Lieder, A. A. Pasternak, E. O. Lieder, W. Gast, G. de Angelis, and D. Bazzacco, *Eur. Phys. J. A* **47**, 115 (2011).
- [32] D. Jerrestam, B. Fogelberg, R. A. Bark, I. G. Bearden, G. Sletten, W. Klamra, J. Cederkäll, S. Mitarai, T. Shizuma, and E. Mäkelä, *Phys. Rev. C* **52**, 2448 (1995).
- [33] A. Görgen, R. M. Clark, P. Fallon, M. Cromaz, M. A. Deleplanque, R. M. Diamond, G. J. Lane, I. Y. Lee, A. O. Macchiavelli, R. G. Ramos, F. S. Stephens, C. E. Svensson, K. Vetter, D. Ward, M. P. Carpenter, R. V. F. Janssens, and R. Wadsworth, *Phys. Rev. C* **65**, 027302 (2002).
- [34] E. O. Lieder, A. A. Pasternak, R. M. Lieder, R. A. Bark, E. A. Lawrie, J. J. Lawrie, S. M. Mullins, S. H. T. Murray, S. S. Ntshangase, P. Papka, N. Kheswa, W. J. Przybyłowicz, P. T. Sechogela, and K. O. Zell, *Nucl. Instrum. Methods Phys. Res., Sect. A* **607**, 591 (2009).
- [35] R. Bengtsson and S. Frauendorf, *Nucl. Phys. A* **327**, 139 (1979).
- [36] F. A. Rickey, J. A. Grau, L. E. Samuelson, and P. C. Simms, *Phys. Rev. C* **15**, 1530 (1977).
- [37] A. O. Macchiavelli, J. Burde, R. M. Diamond, C. W. Beausang, M. A. Deleplanque, R. J. McDonald, F. S. Stephens, and J. E. Draper, *Phys. Rev. C* **38**, 1088(R) (1988).
- [38] D. Jerrestam, F. Lidén, J. Gizon, L. Hildingsson, W. Klamra, R. Wyss, D. Barnéoud, J. Kownacki, Th. Lindblad, and J. Nyberg, *Nucl. Phys. A* **545**, 835 (1992).
- [39] H.-J. Keller, S. Frauendorf, U. Hagemann, L. Käubler, H. Prade, and F. Sary, *Nucl. Phys. A* **444**, 261 (1985).
- [40] J. Meng, J. Peng, S. Q. Zhang, and S.-G. Zhou, *Phys. Rev. C* **73**, 037303 (2006).
- [41] J. Peng, H. Sagawa, S. Q. Zhang, J. M. Yao, Y. Zhang, and J. Meng, *Phys. Rev. C* **77**, 024309 (2008).
- [42] J. M. Yao, B. Qi, S. Q. Zhang, J. Peng, S. Y. Wang, and J. Meng, *Phys. Rev. C* **79**, 067302 (2009).
- [43] J. Li, S. Q. Zhang, and J. Meng, *Phys. Rev. C* **83**, 037301 (2011).
- [44] A. D. Ayangeakaa *et al.*, *Phys. Rev. Lett.* **110**, 172504 (2013).
- [45] P. W. Zhao, Z. P. Li, J. M. Yao, and J. Meng, *Phys. Rev. C* **82**, 054319 (2010).
- [46] B. Qi, S. Q. Zhang, S. Y. Wang, J. M. Yao, and J. Meng, *Phys. Rev. C* **79**, 041302(R) (2009).